Electrohydrodynamic instabilities in microchannels with time periodic forcing

David A. Boy and Brian D. Storey
Franklin W. Olin College of Engineering, Needham, Massachusetts 02492, USA
(Received 31 January 2007; revised manuscript received 17 April 2007; published 10 August 2007)

In microfluidic applications it has been observed that flows with spatial gradients in electrical conductivity are unstable under the application of sufficiently strong electric fields. These electrohydrodynamic instabilities can drive a nonlinear flow despite the low Reynolds number. Such flows hold promise as a simple mechanism for mixing fluids. In this work, the effect of a time periodic electric field on the instability is explored. The case where an electric field is applied across a diffuse interface of two fluids with varying electrical conductivity is considered. Frequency-dependent behavior is found only in the regime where the instability growth rates are very slow and cannot outpace mixing by molecular diffusion. Improving mixing by modulation of the electric body force is not a viable strategy in this geometry.

DOI: 10.1103/PhysRevE.76.026304 PACS number(s): 47.20.−k, 47.65.−d

I. INTRODUCTION

Over the past 15 years there has been extensive research into designing microfluidic systems to perform biological and chemical analysis on integrated microchips. These devices offer the promise of integrating many laboratory processes onto a single chip, thereby increasing throughput and decreasing assay cost [1]. Many applications require mixing fluids, which has long been identified as a key challenge for microfluidics. The challenge is that viscosity dominates at the microscale and mixing by natural inertia-driven turbulence is not possible. While momentum diffusion acts quickly over microscopic length scales, molecular diffusion is often prohibitively slow. The slow rate of molecular diffusion is especially problematic in solutions containing large macromolecules. Numerous passive and active mixing strategies have been proposed to overcome this challenge [2,3].

Recent work has investigated a mixing strategy that uses electrohydrodynamic (EHD) instabilities to achieve nonlinear, microchannel flow. It has been known for some time that EHD instabilities can occur when electric fields are applied to fluids with spatial gradients in their electrical properties [4–6]. Of interest to the present work are instabilities occurring from the interaction of applied electric fields and fluid electrical conductivity gradients. These conductivity gradient instabilities were studied extensively by Melcher and coauthors [7–10]. Fluid conductivity gradients couple with applied electric fields to generate charge in the bulk fluid. The applied electric field can exert a destabilizing body force on the charged fluid. If this force exceeds a critical strength where diffusion can no longer stabilize the flow, then instability ensues.

Electrokinetic flows with fluid conductivity gradients are critical to applications such as field amplified sample stacking, isoelectric focusing, and electrophoretic assays where sample and buffer conductivities are uncontrolled. Electrohydrodynamic instabilities have been studied in the context of these microfluidic geometries and applications. Baygents and Baldessari studied an electric field applied across a thin fluid layer with linearly varying conductivity as a model for isoelectric focusing [11]. Lin *et al.* experimentally studied the instability of a diffuse interface of two fluids of different conductivity with an electric field applied parallel to the interface [12]. They found agreement between experiments, analysis, and simulations demonstrating the basic physical mechanisms as described by Hoburg and Melcher were valid in the microfluidic regime [7]. Chen *et al.* studied convective and absolute instability occurring at the interface of two fluids merging at a *T* junction [13]. They also found agreement between analysis and experiments, validating the interpretation of the basic physical mechanisms. El Moctar *et al.* designed a rapid micromixer that relied upon a voltage applied across a diffuse interface of two fluids with different electrical properties [14]. Their experiments clearly show a dramatic change from laminar to nonlinear flow upon application of an electric field. The slow rate of molecular diffusion normally causes mixing problems in microfluidics. In these unstable EHD flows, however, the slow rate of diffusion is the origin of nonlinear flow. Small spatial structures in fluid conductivity persist and it is from these small scale conductivity gradients that the destabilizing body forces arise [15].

Experimental results have shown that electrokinetic mixing can be improved by adding a time periodic component to the driving electric field [16]. Recent experimental work by Shin *et al.* showed that a cross-junction instability has a resonant effect when a periodic component was added to the driving electric field [17]. In the experiments of Shin *et al.*, the flow is forced with a time periodic component of the electric field that enhances growth rates of interfacial waves, which originate from the junction. They found an optimal frequency for enhanced mixing.

The idea of using time periodic forcing to enhance convective transport is common in heat transfer applications [18,19]. It has been observed that an optimal frequency for heat transfer enhancement exists in many applications due to resonance with the hydrodynamics. In addition to enhancing transport, time periodic forcing can have a major impact on flow stability. The mathematical foundations for studying hydrodynamic stability of periodically forced flows have been well developed, and details can be found in Von Kerczek and Davis [20]. Recently, stability of time modulated electrokinetic microflows has received attention from Suresh and Homsy [21] and Chang and Homsy [22].

The goal of this paper is to explore the role that time periodic electrical forcing has on EHD instabilities in micro-

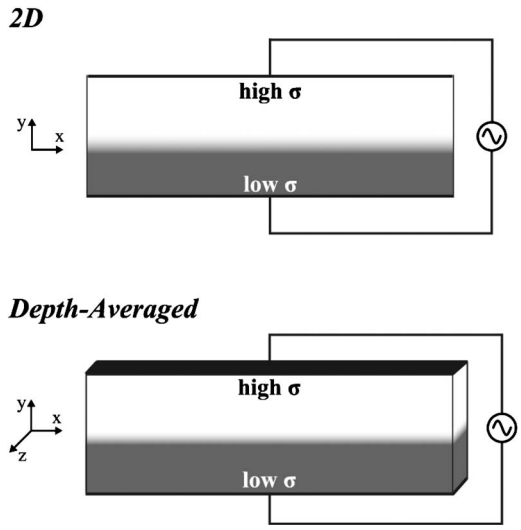

FIG. 1. Basic configuration of interest to this study. We are interested in two physical geometries: an infinitely deep 2D fluid layer and a shallow channel. For modeling flow in the shallow channel we will use a set of depth-averaged equations that were developed in previous work [24]. The initial assumed conductivity profile is shown as a high conductivity fluid above a low conductivity fluid.

channels. Specifically, we are motivated by the problem of finding enhanced mixing by adding an optimal frequency component that modulates the electric body force. We are further motivated by the fact that in many experiments, such as those by El Moctar *et al.* [14], alternating current (ac) is used to reduce bubble formation from electrolysis. In these cases it is important to understand stability of electrohydrodynamic systems under ac forcing. While we have found that a time periodic electric field can have a major impact on flow stability, we have not found a case where control of mixing rates is achieved by simple adjustment of the frequency.

The configuration of interest is a 2D fluid layer bounded between two solid walls and assumed to be periodic down the length of the channel. The upper half of the channel contains a high conductivity fluid while the lower half contains a low conductivity fluid while a voltage is applied across the fluid layer. We investigate this case using two equation sets; one set assumes the flow is purely two dimensional, and the other set considers the microchannel to be shallow. The shallow channel geometry has a set of governing equations that are averaged across the channel depth resulting in a set of two-dimensional equations that account for three-dimensional geometry. The geometries of interest are shown in Fig. 1.

II. GOVERNING EQUATIONS

In an earlier work, a set of governing equations suitable for the study of electrokinetic instabilities in microchannels was developed [12]. The governing equations are conservation of mass for a two species symmetric electrolyte solution, Poisson's equation for the electric field, conservation of mass for an incompressible liquid, and conservation of momentum including the body force due to an electric field. Our equations are reduced from the more general ion transport equations [23]. Our reduced equations make the assumptions that charge relaxes instantaneously compared to the rate of change of conductivity due to advection and that the difference in cationic and anionic concentrations is small compared to the background concentration. Further, we assume a symmetric, binary electrolyte, which allows us to use conductivity and charge density as variables as opposed to tracking molar concentration of individual species. Details on the derivations and applicability of the model equations can be found in the literature [12]. We simply list the governing equations as

$$\frac{\partial \sigma}{\partial t} + \mathbf{v} \cdot \nabla \sigma = D \nabla^2 \sigma, \tag{1}$$

$$\nabla \cdot (\sigma \nabla \Phi) = 0, \tag{2}$$

$$\epsilon \nabla^2 \Phi = -\rho_E, \tag{3}$$

$$\nabla \cdot \mathbf{v} = 0, \tag{4}$$

$$\rho \left(\frac{\partial \mathbf{v}}{\partial t} + \mathbf{v} \cdot \nabla \mathbf{v} \right) = -\nabla p + \mu \nabla^2 \mathbf{v} - \rho_E \nabla \Phi. \tag{5}$$

Here σ is the electric conductivity, D is the diffusivity of the conductivity field, $\mathbf{v}$ is the velocity field, Φ is the electric potential, ϵ is the permittivity of the buffer, ρ_E is the charge density, ρ is the buffer liquid density, p is the pressure, and μ is the liquid viscosity. Equations (1)–(5) represent the conservation of conductivity, current continuity, Poisson's equation for the electric potential, conservation of mass for an incompressible fluid, and conservation of momentum, respectively.

The derivation of the above equations relies upon the fact that the fluid bulk is essentially electroneutral. The difference in anionic to cationic concentration relative to the bulk concentration $\Delta C_0 / C_0$ for our application can be estimated as

$$\frac{\Delta C_0}{C_0} = \frac{\epsilon \Phi_0}{F C_0 H} \sim 10^{-4} - 10^{-7}, \tag{6}$$

indicating that we are safely in the electroneutral regime. Above, Φ_0 is the applied potential across the fluid layer, F is Faraday's constant, H is the channel half width (in the y direction), and C_0 is the bulk concentration. It is this assumption of electroneutrality that results in ohmic current strongly dominating over diffusive current. The assumption of instantaneous charge relaxation holds when the ratio of the charge relaxation time to electroviscous time (defined in the next section) is small. For our application we estimate this ratio to be

$$\frac{t_{\text{charge}}}{t_{ev}} = \frac{\epsilon / \sigma}{\mu H^2 / (\epsilon \Phi_0^2)} \sim 10^{-2} - 10^{-6}, \tag{7}$$

indicating that our assumption is valid. The assumption of instantaneous charge relaxation is also expected to break down once the forcing frequency becomes fast relative to the

charge relaxation time. The forcing frequency f should satisfy the relation $f \ll \sigma/\epsilon$ in order to safely make the assumption. Further details on the validity of the equations and an explanation of the above scaling arguments can be found in Lin *et al.* [12].

It is important to note that Eqs. (1)–(5) are only valid for the bulk fluid region outside the electric double layer and will not account for electrode screening. Such screening effects can easily be accounted for in the analysis, but we will show that their inclusion does not effect the basic conclusions of this paper.

III. ANALYSIS

We start by nondimensionalizing the governing equations with the following scales:

$$[x,y] = H, \quad [\Phi] = \Phi_0, \quad [\sigma] = \sigma_0, \quad [u,v] = U_{ev} \equiv \frac{\epsilon \Phi_0^2}{H\mu},$$

$$[t] = t_{ev} = \frac{H}{U_{ev}}, \quad [P] = \rho U_{ev}^2, \quad [\rho_E] = \frac{\epsilon \Phi_0}{H^2},$$

where σ_0 is the conductivity of the lower half of the channel and Φ_0 is the root-mean-squared (RMS) value of the potential applied across the fluid layer. The velocity scale, the electroviscous velocity U_{ev}, is set such that viscous forces balance electrical body forces [12].

The first equation set that we will study is the 2D projection of the governing equations. Storey showed that while an initial 2D conductivity profile will result in 3D flow, a 2D approximation is still useful to capture the basic instability mechanisms and threshold [15]. The 2D approximation predicts instability to occur at much lower electric fields than found experimentally in thin microchannels [12]. Using the simulation methods from previous work [15], we confirmed the instability threshold predicted with the 2D equations is reasonably accurate when compared to 3D direct numerical simulations of channels with square cross section. We expect the 2D analysis to provide the lower bound for stability in 3D channels.

In two dimensions it is convenient to use the vorticity-stream function form of the Navier-Stokes equations. We can also remove the charge density from the formulation by substituting Eq. (3) into the momentum equation. Making the appropriate substitutions yields a set of nondimensionalized, 2D equations for the x-y plane,

$$\frac{\partial \sigma}{\partial t} + \mathbf{v} \cdot \nabla \sigma = \frac{1}{\mathrm{Ra}} \nabla^2 \sigma, \tag{8}$$

$$\nabla \cdot (\sigma \nabla \Phi) = 0, \tag{9}$$

$$\frac{\partial \omega}{\partial t} + \mathbf{v} \cdot \nabla \omega = \frac{1}{\mathrm{Re}} [\nabla^2 \omega + \nabla (\nabla^2 \Phi) \times \nabla \Phi], \tag{10}$$

$$\nabla^2 \Psi = -\omega, \tag{11}$$

where ω is the z component of the vorticity, Ψ is the stream function, and the stream function is related to velocity in the usual manner.

There are two dimensionless parameters that emerge in this analysis: Reynolds number Re, and electric Rayleigh number Ra,

$$\mathrm{Re} \equiv \frac{\rho U_{ev} H}{\mu} \equiv \frac{\rho \epsilon \Phi_0^2}{\mu^2}, \quad \mathrm{Sc} \equiv \frac{\mu}{\rho D}, \quad \mathrm{Ra} \equiv \mathrm{Re}\,\mathrm{Sc}.$$

These two parameters are related to each other through the Schmidt number Sc, which is a fluid property. The Schmidt number is set to 500 throughout this paper based on the experimental parameters used by Lin *et al.* [12]. A Schmidt number of 500 is typical of low molecular weight, aqueous electrolytes. The Rayleigh number is the most important parameter for determining stability, and variation of the Schmidt number has little impact on the final results. We checked a variety of cases with larger Schmidt numbers to confirm that the Rayleigh number is the key parameter. Also, as long as the Reynolds number is relatively low, its value has little impact on stability. In the limit of zero Reynolds number, the Stokes equations apply, and the Rayleigh number becomes the *only* dimensionless parameter.

Boundary conditions at the upper and lower channel wall are no flux of conductivity, no normal velocity, and no fluid slip. The potential boundary condition is Dirichlet. The velocity boundary conditions are applied to the stream function, which is subjected to boundary conditions $\Psi = 0$ and $\partial \Psi / \partial y = 0$ at the walls. It is important to note that we will be neglecting electro-osmotic flow effects throughout this analysis. It was found in previous work to have little influence over stability behavior when the ratio of electro-osmotic to electroviscous velocity is small [12,13]. Neglecting electro-osmotic flow reduces the number of free parameters that the system depends upon and simplifies the presentation of results. This assumption is revisited in the Discussion section.

The second equation set we will study is appropriate for modeling flow in microchannels with shallow aspect ratios (see Fig. 1). Flow in these shallow channels is significantly different than flow in a 2D fluid layer [24,25]. Storey *et al.* used a zeroth-order Hele-Shaw analysis to derive a set of depth-averaged equations [24]. By taking advantage of the channel's small aspect ratio and integrating the governing equations across the z direction, Storey *et al.* were able to derive a 2D equation set for flow in the x-y plane. A later paper carried this Hele-Shaw analysis to higher order [25]. That set of equations was found to more accurately model the nonlinear flow and accounted for conductivity dispersion. The important feature of these depth-averaged equations is that a 2D equation set can formally account for viscous effects across the shallow third dimension.

The derivation of the depth-averaged equations is lengthy and details are found in Refs. [24,25]. To be consistent with our previous analysis, we take the electro-osmotic velocity to be zero; this assumption simplifies the dispersion effect

within the governing depth-averaged equations. The higher order depth-averaged equations in dimensionless form are [25]

$$\frac{\partial \sigma}{\partial t} + \mathbf{v} \cdot \boldsymbol{\nabla} \sigma = \frac{1}{\delta^2 \, \mathrm{Ra}} \left\{ \nabla^2 \sigma + \frac{2}{105} \mathrm{Ra}^2 \, \delta^4 \, \boldsymbol{\nabla} \cdot [\mathbf{v}(\mathbf{v} \cdot \boldsymbol{\nabla} \sigma)] \right\}, \tag{12}$$

$$\boldsymbol{\nabla} \cdot (\sigma \nabla \Phi) = 0, \tag{13}$$

$$\delta^2 \left(\frac{\partial \omega}{\partial t} + \mathbf{v} \cdot \boldsymbol{\nabla} \omega \right) = \frac{1}{\delta^2 \, \mathrm{Re}} \{ \nabla (\nabla^2 \Phi) \times \nabla \Phi - 3\omega + \delta^2 \nabla^2 \omega \}, \tag{14}$$

$$\nabla^2 \Psi = -\omega, \tag{15}$$

where $\delta = d/H$ and d is the channel half-depth in the z direction. The dimensionless parameters are exactly as before except that velocity is scaled as $\delta^2 U_{ev}$. The definitions of the Reynolds and Rayleigh numbers remain the same. The boundary conditions at the upper and lower channel walls are identical to the 2D equations.

The first set, Eqs. (8)–(11), will be referred to as the 2D equations. These equations take only a 2D component of the fundamental flow equations and assume the fluid layer is infinitely deep and invariant in the z direction. The second equation set, Eqs. (12)–(15), will be referred to as the depth-averaged equations. The depth-averaged equations have taken an integrated average over the shallow depth (z direction) of the channel. The depth-averaging operation accounts for 3D effects but results in a 2D equation set.

A. Linearized equations

To study the effect of time periodic electric fields on stability, we linearize the governing equations about a base state. The base state is assumed to be only a function of y. We start with a conductivity profile that would result from instantly placing two fluids into contact and allowing the interface to diffuse for a short time. We assume that the conductivity profile is steady thereafter. Ramifications of this quasisteady assumption are explained in detail in the Results section. Once the conductivity profile is known, we can compute the base state for the electric potential from current continuity. The base state velocity is zero. To perform the linearization, we assume solutions composed of a zeroth-order base state and a spatially periodic small perturbation, i.e., $f = f_0 + \epsilon f_1(t,y) e^{ikx}$. The above substitution is made in the governing equations, and like powers of ϵ are collected. The linearization procedure is straightforward, and we only present the final result.

The base state for electric potential is found by integrating the zeroth-order current continuity equation,

$$\frac{d}{dy} \left(\sigma_0 \frac{d\Phi_0}{dy} \right) = 0, \tag{16}$$

using the boundary condition that the lower boundary is always held at zero potential and the upper boundary varies as $\sqrt{2}\cos(ft)$ such that $\Phi_0(t,y) = \sqrt{2}\Phi_0(y)\cos(ft)$. By using the RMS value as the scale for electric potential, the ac and dc cases will converge in the high frequency limit.

The equations for the first-order perturbation to the base state with the 2D equations are (we drop the subscript 1 for simplicity)

$$\frac{\partial \sigma}{\partial t} = ik\Psi \frac{d\sigma_0}{dy} + \frac{1}{\mathrm{Ra}} \nabla^2 \sigma, \tag{17}$$

$$\frac{d\sigma_0}{dy} \frac{\partial \Phi}{\partial y} + \sigma_0 \nabla^2 \Phi + \sqrt{2} \left(\frac{d\Phi_0}{dy} \frac{\partial \sigma}{\partial y} + \sigma \frac{d^2 \Phi_0}{dy^2} \right) \cos(ft) = 0, \tag{18}$$

$$\frac{\partial \nabla^2 \Psi}{\partial t} = \frac{1}{\mathrm{Re}} \left\{ \nabla^4 \Psi + \sqrt{2} \left(ik\Phi \frac{d^3 \Phi_0}{dy^3} - ik\nabla^2 \Phi \frac{d\Phi_0}{dy} \right) \cos(ft) \right\}. \tag{19}$$

The equations for the first-order perturbation to the base state with the depth-averaged equations are

$$\frac{\partial \sigma}{\partial t} = ik\Psi \frac{d\sigma_0}{dy} + \frac{1}{\delta^2 \, \mathrm{Ra}} \nabla^2 \sigma, \tag{20}$$

$$\frac{d\sigma_0}{dy} \frac{\partial \Phi}{\partial y} + \sigma_0 \nabla^2 \Phi + \sqrt{2} \left(\frac{d\Phi_0}{dy} \frac{\partial \sigma}{\partial y} + \sigma \frac{d^2 \Phi_0}{dy^2} \right) \cos(ft) = 0, \tag{21}$$

$$\delta^2 \frac{\partial \nabla^2 \Psi}{\partial t} = \frac{1}{\delta^2 \, \mathrm{Re}} \left\{ \delta^2 \nabla^4 \Psi - 3\nabla^2 \Psi + \sqrt{2} \left(ik\Phi \frac{d^3 \Phi_0}{dy^3} - ik\nabla^2 \Phi \frac{d\Phi_0}{dy} \right) \cos(ft) \right\}. \tag{22}$$

B. Galerkin expansion

Following the work of Von Kerczek, who analyzed periodically forced Stokes boundary layers, we use the Galerkin approach to write the equations as a set of ordinary differential equations for the coefficients to a set of basis functions [20]. We expand the variables as a series of basis functions that naturally satisfy the boundary conditions,

$$\Psi = \sum_{n=1}^{N} f_n(t) \Psi_n(y), \quad \sigma = \sum_{n=0}^{N-1} g_n(t) \sigma_n(y), \tag{23}$$

$$\Phi = \sum_{n=1}^{N} h_n(t) \Phi_n(y).$$

For the stream function we use solutions of the eigenvalue problem,

$$\left(\frac{d^2}{dy^2} - k^2 \right)^2 \Psi_n = -\lambda_n^2 \left(\frac{d^2}{dy^2} - k^2 \right) \Psi_n, \tag{24}$$

subjected to clamped boundary conditions as our basis functions [26]. The basis functions for the conductivity are

$$\sigma_n = C_n \cos\left(\frac{y+1}{2} n\pi\right), \tag{25}$$

where $C_n = 1/\sqrt{2}$ for $n=0$ and $C_n = 1$ otherwise. The basis functions for the potential are

$$\Phi_n = \sin\left(\frac{y+1}{2} n\pi\right). \tag{26}$$

We proceed in the usual manner where we take an inner product, $\langle a,b\rangle = \int_{-1}^{1} abdy$, of the four sets of linearized equations with the appropriate basis functions. From our definitions,

$$I = \langle \Phi_n, \Phi_m \rangle = \langle \sigma_n, \sigma_m \rangle, \quad J = \langle \Psi_n, \Psi_m \rangle,$$

where I is the identity matrix.

Straightforward calculation yields the final matrix form of the ordinary differential equations for the vector of coefficients $\mathbf{f}$ and $\mathbf{g}$,

$$\frac{d\mathbf{x}}{dt} = \Gamma(t)\mathbf{x}, \tag{27}$$

where the vector components of $\mathbf{x}$ are $\mathbf{x}_1 = \mathbf{f}$ and $\mathbf{x}_2 = \mathbf{g}$.

The matrix components of Γ with the 2D equation set are

$$\Gamma_{11,2D} = \frac{1}{\mathrm{Re}}(R - k^2 J)^{-1}(S - 2k^2 R + k^4 J), \tag{28}$$

$$\Gamma_{12,2D} = \frac{-i2k}{\mathrm{Re}}(R - k^2 J)^{-1} T(A^{-1}B)\cos^2(ft), \tag{29}$$

$$\Gamma_{21,2D} = ikP, \tag{30}$$

$$\Gamma_{22,2D} = \frac{1}{\mathrm{Ra}}(Q - k^2 I). \tag{31}$$

The matrix components of Γ computed with the depth-averaged equation set are related to those computed with the 2D equation set as follows:

$$\Gamma_{11,DA} = -\frac{3}{\delta^4 \mathrm{Re}} I + \frac{1}{\delta^2}\Gamma_{11,2D}, \tag{32}$$

$$\Gamma_{12,DA} = \frac{1}{\delta^4}\Gamma_{12,2D}, \tag{33}$$

$$\Gamma_{21,DA} = \Gamma_{21,2D}, \tag{34}$$

$$\Gamma_{22,DA} = \frac{1}{\delta^2}\Gamma_{22,2D}. \tag{35}$$

The components matrices of Γ are defined as follows:

$$P = \left\langle \frac{d\sigma_0}{dy}\Psi_n, \sigma_m \right\rangle, \quad Q = \left\langle \frac{d^2\sigma_n}{dy}, \sigma_m \right\rangle,$$

$$R = \left\langle \frac{d^2\Psi_n}{dy^2}, \Psi_m \right\rangle, \quad S = \left\langle \frac{d^4\Psi_n}{dy^4}, \Psi_m \right\rangle,$$

$$A = \left\langle \frac{d\sigma_0}{dy}\frac{d\Phi_n}{dy} + \sigma_0\left(\frac{d^2}{dy^2} - k^2\right)\Phi_n, \Phi_m \right\rangle, \tag{36}$$

$$B = \left\langle \frac{d\Phi_0}{dy}\frac{d\sigma_n}{dy} + \frac{d^2\Phi_0}{dy^2}\sigma_n, \Phi_m \right\rangle,$$

$$T = \left\langle -\frac{d\Phi_0}{dy}\left(\frac{d^2}{dy^2} - k^2\right)\Phi_n + \frac{d^3\Phi_0}{dy^3}\Phi_n, \Psi_m \right\rangle. \tag{37}$$

The matrices can be computed analytically when the expressions only involve the basis functions themselves [26]. Matrices that involve the base state of conductivity or electric potential must be computed numerically. We found our results are not sensitive to the method or details of numerical integration.

IV. RESULTS

A. Constant electric field (dc)

To predict stability with a constant electric field we set the forcing frequency to zero and compute the eigenvalues of Γ. If the real part of any eigenvalue s is greater than zero then the flow is unstable. The base state of conductivity is assumed to be steady in the analysis. Therefore, we can only consider the solution valid if the disturbance growth rate is fast compared to molecular diffusion of the base state [11,12]. In dimensional units, the time scale for molecular diffusion of the interface is

$$t_{\mathrm{diff}} \sim \frac{(\alpha(t)H)^2}{D}, \tag{38}$$

where $\alpha(t)$ is the dimensionless thickness of the interface, which increases with time. The dimensional time it takes the perturbation to grow by a factor A, is

$$t_{\mathrm{grow}} \sim \frac{H\log(A)}{sU_{ev}}, \tag{39}$$

where H/U_{ev} is the nondimensional time scale. Our quasi-steady solution is valid when

$$\frac{t_{\mathrm{diff}}}{t_{\mathrm{grow}}} = \frac{s_r\alpha^2 H U_{ev}}{\log(A)D} = \frac{s_r\alpha^2\,\mathrm{Ra}}{\log(A)} \gg 1. \tag{40}$$

For the initial interface that we are considering, the thickness is approximately $\alpha = 0.2$. To determine where our solution is valid, we apply a conservative estimate and look where the amplitude of the disturbance grows by $A = 10\,000$ before significant diffusion of the base state occurs. Using this criteria the solution assuming a steady base state of conductivity is clearly valid when

$$s\,\mathrm{Ra} > 250. \tag{41}$$

When $s\,\mathrm{Ra} > 250$ we expect our linear analysis to be valid and the instability to be very strong relative to molecular diffusion, representing a region where mixing is quite vigorous. When $0 < s\,\mathrm{Ra} < 250$, the flow may be unstable but we must use caution when interpreting the results of the analysis that assumes a steady base state.

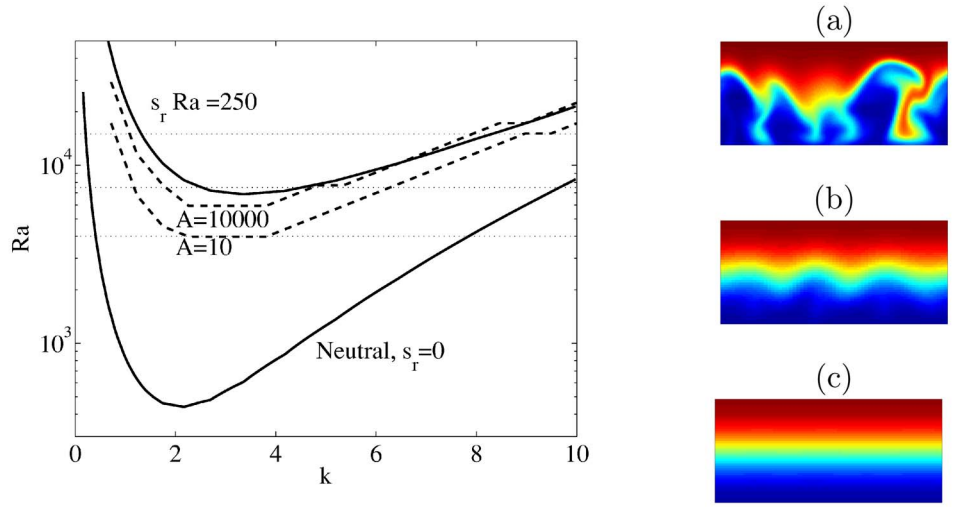

FIG. 2. (Color online) Linear stability diagram with the 2D equation set and a conductivity ratio of 10:1. Solid contours of s Ra are shown for values of 0 and 250 computed with a steady base state. Two dashed contours show results from the simulation with a transient base state. The curves shown are for amplification factors of $A=10$ and $A=10\,000$. Snapshots of the conductivity field computed from nonlinear simulations are shown at values of Ra=4000, 7500, and 15 000 in (a), (b), and (c), respectively. The three dotted lines on the contour plot show these values of Ra. We can use this figure to classify different regimes of the flow. For Ra$\gg$6000 we observe the flow to be unstable and therefore to have strong mixing. For Ra$\sim$6000 we observe unstable waves in the conductivity field but not strong folding and mixing. For 4000$<$Ra$<$6000 we observe some flow with perhaps only slightly observable waves. For Ra$<$4000 we find the perturbation to the initial state will only grow by a factor of 10 before the conductivity field simply diffuses away.

We can also compute whether the flow will be unstable with a transient base state by directly solving the time-dependent linearized equations using Chebyshev pseudospectral methods [27]. The numerical methods are similar to those discussed by Lin *et al.* [12]. Our procedure takes the fastest growing eigenfunction for a given base state as the initial perturbation. We then simultaneously integrate forward in time the equations governing the zeroth-order base state and the first-order perturbation. We observe that the perturbation will exponentially grow in amplitude, reach a maximum value, and then begin to decay as the initial conductivity gradient (and driving force for the instability) diffuses away. We can certainly consider a flow unstable if the perturbation reaches a maximum amplification of 10 000. Again, the selection of 10 000 as the necessary criteria is a very conservative one and selecting different amplification criteria does not change our basic results. The reason that we do not use the Galerkin procedure to integrate the equations forward in time [i.e., Eq. (27)] is that Γ depends upon the base state and would need to be recomputed at every time step. In addition, having alternate numerical methods for the same problem provides us with additional validation of our results.

Figure 2 shows stability results at a conductivity ratio of 10:1 with the 2D equation set. The solid contours show values of s Ra=0 and s Ra=250 as a function of Ra and wave number k. The solid lines are computed from the eigenvalues of Γ. The dashed contours show results from integrating the linearized equations accounting for the transient base state as described above. We show contours where the maximum amplitude of the disturbance is $A=10$ and $A=10\,000$. The transient analysis agrees with our scaling argument based upon competition of time scales for diffusion and perturbation growth; the curve for s Ra=250 is similar to the curve of $A=10\,000$. Figure 2 demonstrates that the time scale argument applied to results obtained with a steady base state is reasonable. This result is important as it will allow us to interpret the stability results obtained when the system is under ac forcing.

To further confirm our interpretation and linear stability analysis, we perform a direct numerical simulation of Eqs. (6)–(9). Snapshots from the simulation are shown in the images of Fig. 2 and details of the simulation methods were discussed by Lin *et al.* [12]. Figure 2 shows that below Ra <460, the flow is linearly stable. In the region 460$<$Ra <4000 the flow is unstable when the base state is considered steady. However, our simulations and analysis show that instability growth rates are overwhelmed by molecular diffusion of the base state in this region. The perturbation will only grow by a factor of 10 ($A=10$), at most, before molecular diffusion eliminates the initial conductivity gradient as shown by the lower dashed curve. In the region 4000$<$Ra <6000 the flow is unstable, but the direct numerical simulations predict a weak flow that cannot significantly deform the conductivity field. The exact magnitude of the flow velocity depends upon the assumed disturbance amplitude, but strong mixing does not occur. Close to Ra$\sim$6000, simulations begin to show observable waves in the conductivity field. Well above Ra$>$6000 the flow quickly becomes well mixed. We therefore interpret the results such that strong and rapid mixing is expected when s Ra$>$250. Below s Ra <250 instability may be observed but it is insufficient for micromixer design. While the criteria for mixing cannot be precise, we will show that in the case of the time periodic forcing the exact criteria will not influence the basic conclusions of this paper. Similar scaling arguments were used by

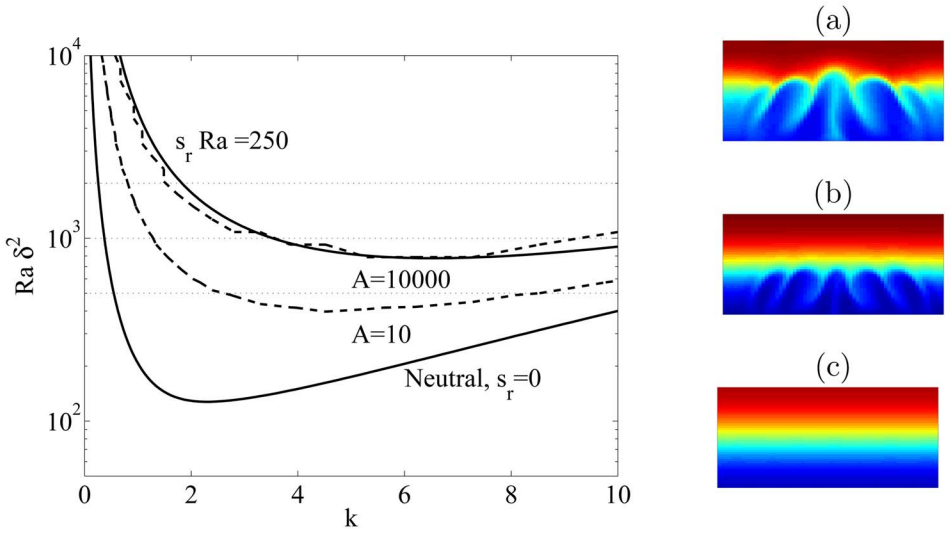

FIG. 3. (Color online) Linear stability diagram with the depth-averaged equation set and a conductivity ratio of 10:1. Solid contours of s Ra are shown for values of 0 and 250 computed with a steady base state. The two dashed contours show results from simulations with a transient base state. The curves shown are for amplification factors of $A=10$ and $A=10\,000$. Snapshots of the conductivity field computed from nonlinear simulations are shown at values of Ra=2000, 1000, and 500 in (a), (b), and (c), respectively. The dotted lines on the contour plot indicate these values of Ra. We can use this figure to classify different regimes of the flow. For Ra $\delta^2 \gg 800$ we observe the flow to be unstable and therefore to have strong mixing. For Ra $\delta^2 \sim 800$ we observe unstable waves in the conductivity field but not strong folding and mixing. For $400 <$ Ra $\delta^2 < 800$ we observe some flow with perhaps slightly observable waves. For Ra $\delta^2 < 400$ we find the perturbation to the initial state will only grow by a factor of 10 before the conductivity field simply diffuses away.

Lin *et al.* and the interpretation was experimentally validated for a slightly different geometry.

The results of stability analysis conducted with the depth-averaged equation set are summarized in Fig. 3 for a conductivity ratio of 10:1. Figure 3 shows contours of s Ra, the stability boundary based on integrating the linearized equations accounting for a transient base state, and snapshots of nonlinear simulations at selected Rayleigh numbers. The interpretation is exactly as before. The reader should note that the y axis is Ra δ^2. For a thin channel with $\delta=0.1$, the y axis would be multiplied by 100 to obtain a Rayleigh number to compare to Fig. 2. Comparing Fig. 2 to Fig. 3 we find the shallow channel flow is much more stable than the 2D channel, in agreement with previous experimental work [12]. The basic stability behavior with the depth-averaged equation set is similar to the 2D equation set, however, the snapshots of conductivity field show significantly different flow. The obvious difference is high wave numbers dominate in the depth-averaged simulations. The emergence of high wave numbers is related to the fact that the z direction introduces a new smaller length scale into the analysis.

B. Time periodic forcing (ac)

The methods for time periodic stability analysis are outlined by Von Kerczek and Davis [20]. Equation (27) is written as a matrix equation,

$$\frac{dF}{dt} = \Gamma(t)F, \tag{42}$$

where $F(t=0)$ is the identity matrix. Equation (42) is numerically integrated for one period of the forcing and the eigenvalues μ of the matrix $F(t=2\pi/f)$ are computed. The Floquet exponent is defined as $\lambda=\log(\mu)/2\pi$, which provides the amount of amplification from one forcing cycle to the next. Since the time scale is not normalized by frequency, we plot contours of the effective growth rate $s=\lambda f$. This growth rate allows us to directly compare the periodically forced case with the dc case. In the periodically forced problem there is a mean growth rate e^{st}, in addition to the oscillatory component. Our analysis of time periodic forcing does not account for the transient, diffusing base state of electrical conductivity. We know from the dc situation that at sufficiently high Rayleigh numbers the quasisteady assumption is accurate and fails near $s=0$.

In the figures that follow, we do not use the electroviscous time scale to scale the frequency. While the electroviscous scale works well for the dc problem (see Lin *et al.* for a detailed discussion), it is not appropriate for scaling frequency in the ac problem. From a balance of electrical and inertial forces we can derive the electroinertial time scale to be $t_{ei}=\sqrt{t_{ev}t_v}$, where $t_{ev}=H/U_{ev}$ is the electroviscous time and $t_v=H^2/v$ is the momentum diffusion time. Recognizing that diffusion of conductivity is the important time scale $t_D=H^2/D$, we arrive at the time scale $\sqrt{t_{ev}t_D}$. We found this time scale more appropriate for scaling frequency. The dimensionless frequency used throughout our formulation is multiplied by $\sqrt{\text{Ra}}$ to convert to this new scaling. Using this scaling, the flow exhibits frequency dependence around $f\sqrt{\text{Ra}} \sim 1$.

The stability results for a single wave number $k=2.5$, with the 2D equations and time periodic forcing are summarized in Fig. 4. We present the single wave number $k=2.5$, because this mode has relatively rapid growth at all Rayleigh num-

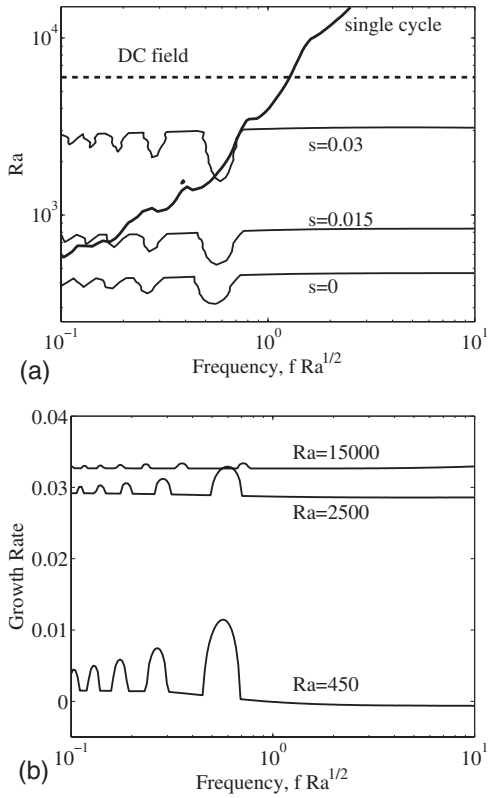

FIG. 4. Stability behavior of the $k=2.5$ mode for a conductivity ratio of 10:1 with the 2D equations. In (a) we show contour lines of growth rate equal to 0, 0.015, and 0.03. We also show the boundary where the flow is unstable in a dc field accounting for a transient base state (dashed line) and the curve above which the flow is unstable in a single forcing cycle. In (b) we show growth rate as a function of frequency at selected Ra.

bers of interest. Results are very similar for other wave numbers. In Fig. 4(a) we show the contour map varying two parameters, Rayleigh number and frequency. In Fig. 4(b) we show the growth rate as a function of frequency for selected Rayleigh numbers. Figure 4(b) is equivalent to holding all parameters constant but varying the frequency. This view shows a clear system resonance. Following the curve for a Rayleigh number of 450 in Fig. 4(b) we find the system is stable at high frequency and then comes unstable as the frequency is lowered and the system passes into its first resonance.

While the system shows a clear frequency dependence, these behaviors are observed in a regime where molecular diffusion of the base state dominates the problem. The analysis of the dc case found good mixing when $\mathrm{Ra}>6000$. This value is denoted by the dashed "dc field" line in Fig. 4(a). Well below this line is where significant system resonance is found. Direct numerical simulations confirm that in the region $\mathrm{Ra}<6000$ simple molecular diffusion of the base state dominates the problem. At higher Rayleigh numbers where instability dominates the problem, we find that the system becomes insensitive to frequency. We see at $\mathrm{Ra}=2500$ in Fig. 4(b), that the frequency dependence already is slight. As Ra is increased further, the response curves show essentially no frequency dependence. Direct numerical simulations of the nonlinear 2D equations were performed at different frequencies for $\mathrm{Ra}=10\,000$ and $\mathrm{Ra}=15\,000$. In all these simulations, a frequency dependence on mixing rates was not observable. Further, we can apply our scaling argument on the competition between diffusion and instability time scale to Fig. 4(b). The peak of the resonance for the $\mathrm{Ra}=450$ would correspond to $s\,\mathrm{Ra}\approx 5$. Our scaling argument would predict that the initial disturbance would amplify by only a factor of $A\approx 1.2$ before the base state was eliminated by molecular diffusion.

On the contour map of Fig. 4(a), we also show a curve that represents the solution blowing up during a single forcing cycle; denoted as "single cycle." If the frequency is low compared to the growth rate, it is possible for perturbations to amplify significantly in a single forcing cycle. Floquet analysis predicts growth from one forcing cycle to the next. The region above the "single cycle" curve is flows where the instability would amplify by a factor of 10 000 in one cycle. If there was interesting frequency-dependent behavior above this curve it also would be unobservable. As discussed previously, molecular diffusion renders the region below the dashed "dc field" line uninteresting for mixing applications. Therefore, we are left with only the upper right portion of Fig. 4(a), where frequency-dependent behavior is observable. The growth rate contours become flat in this region of parameter space.

The usefulness of rescaling frequency is apparent from the fact that resonances occur at approximately the same frequency for different Rayleigh numbers in Fig. 4(a). When scaling frequency by the electroviscous time, the resonances shift to the left as the Rayleigh number is increased. Our analysis shows that growth rate contours become constant at high frequency. This growth rate agrees with the dc analysis corresponding to the same RMS value of electric potential. The agreement between the high frequency ac limit and the dc case provides an additional check on our analysis.

The only practical way to increase the Rayleigh number in a given experiment is to increase the applied potential. If the applied electric potential increases, the time scale will decrease (see Sec. II: Analysis). The contours shown in Fig. 4(a) are dimensionless growth rates. As the Rayleigh number increases, the dimensionless growth rate at high frequency levels off to a constant value. In physical time units, the instability will occur much more rapidly at high electric fields because the time scale has decreased.

In the previous example, we presented a conductivity ratio of 10:1. At a higher conductivity ratio of 100:1 we see similar qualitative behavior, though the frequency dependence becomes more pronounced. Figure 5 presents the same stability information as Fig. 4. At low Ra we find that the frequency dependence is quite dramatic for these high conductivity ratios. The $\mathrm{Ra}=65$ line in Fig. 5(b) shows significant resonance. However, this behavior still occurs in a region where instability time scales are slow enough to be overwhelmed by molecular diffusion of the base state. Resonances are not observable in numerical experiments at even this high conductivity ratio.

We now turn to the depth-averaged equation set. The stability behavior for a conductivity ratio of 10:1 at $k=1.5$ is summarized in Fig. 6. A lower wave number is used for presentation as higher wave numbers have even less pro-

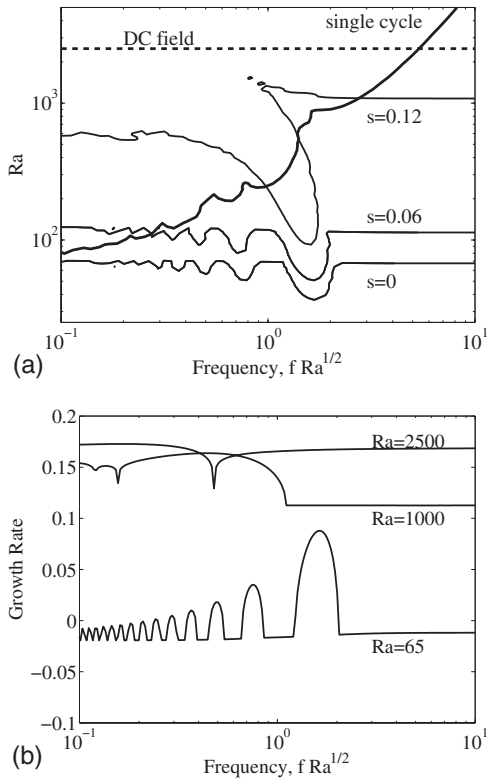

FIG. 5. Stability behavior of the $k=2.5$ mode for a conductivity ratio of 100:1 with the 2D equations. In (a) we show contour lines of growth rate equal to 0, 0.06, and 0.12. We also show the boundary where the flow is unstable in a dc field accounting for a transient base state (dashed line) and the curve above which the flow is unstable in a single forcing cycle. In (b) we show growth rate as a function of frequency at selected Ra.

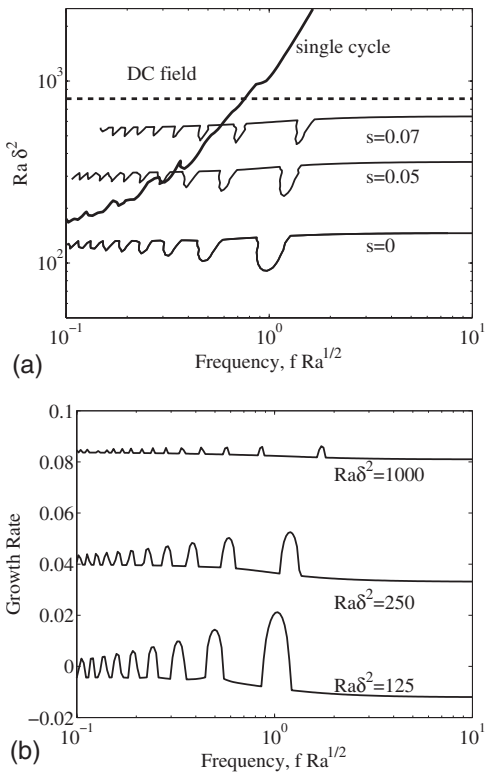

FIG. 6. Stability behavior of the $k=1.5$ mode for a conductivity ratio of 10:1 with the depth-averaged equations. In (a) we show contour lines of growth rate equal to 0, 0.05, and 0.07. We also show the boundary where the flow is unstable in a dc field (dashed line) accounting for a transient base state and the curve above which the flow is unstable in a single forcing cycle. In (b) we show growth rate as a function of frequency at selected Ra.

nounced frequency dependence. Figure 6 shows the same features that we observed with the 2D equation set and the interpretation is identical to Fig. 4. Again, we are not able to find examples with the depth-averaged equations where periodic forcing would have an observable effect on mixing in numerical experiments.

In the preceding figures, we have presented results for selected wave numbers and selected conductivity ratios. The behavior of different wave numbers is similar, and we have chosen to present wave numbers that are among the fastest growing. Results for different wave numbers do not differ significantly in their behavior, nor do they change the basic conclusions of this paper. We explored various conductivity ratios up to 100 and found no new results. We have also explored the high Rayleigh number and high frequency regime outside the regimes presented. We have not yet found a situation of physical parameters where mixing rates can be controlled by varying the frequency.

V. DISCUSSION

Our analysis neglected charging of the double layer at the electrodes. The charging time, as given by Bazant *et al.*, is $t_c=(\lambda/H)\mathrm{Ra}$ in dimensionless units where λ is the Debye length [28]. Neglecting the double layer is valid when the frequency is greater than the inverse charging time for the system $f\sqrt{\mathrm{Ra}}>H/(\lambda\sqrt{\mathrm{Ra}})$. Typical values for λ/H in microfluidic systems can range from 0.01 in small devices with dilute electrolytes to several orders of magnitude smaller in larger systems with concentrated electrolytes. At low frequency, when charging should be accounted for, the double layer capacitance acts as a high-pass *RC* filter on the electric field in the bulk. Double layer charging simply adds another mechanism to reduce instability at low frequency.

Our analysis focused on the bulk instability and neglected electro-osmotic slip at the electrode surface, a valid assumption for ideally polarizable electrodes. Instability due to electro-osmotic slip of the first and second kind has been well studied [29–31]. Such instabilities do not rely upon setting up a bulk conductivity gradient and therefore occur by a different mechanism than the bulk instability we consider. Electro-osmotic instability of the first kind, while possible theoretically, is not feasible for aqueous, inorganic electrolytes [30,31]. Electro-osmotic instability of the second kind occurs only when a current near the limiting value is passing through the system and the double layer takes on a nonequilibrium structure. Such instabilities could occur in our system when there are significant Faradaic reactions at low frequency [31].

While electro-osmotic instability may play a role at low frequency where significant reactions can occur, the analysis is complicated by the fact that the applied voltages typically exceed the thermal voltage 25 mV by a factor of 100 or more. The limits of applicability for the dilute solution equations are well exceeded in such microfluidic applications [32]. Additional atomistic modeling and experimental work is needed on electrochemical flows at large applied voltages before such problems can be fully analyzed.

Thus far, all results have been presented in terms of the dimensionless Rayleigh number. In order to connect to previous and possible future experimental results we can easily convert our results to the physical values. Using physical parameters of water and taking Sc=500, typical of aqueous inorganic electrolytes, we can compute voltages that would achieve the mixing regimes discussed in this work. For the 2D equations, the mixing threshold of Ra=6000 for a 10:1 conductivity ratio corresponds to an applied voltage of approximately 4 V. For the depth-averaged equations in a channel with a 10:1 aspect ratio, the critical dc voltage is approximately 14 V. It is interesting to note that these critical voltages do not depend upon the size of the channel, only the properties of the liquid electrolyte and the initial conductivity ratio. The voltage required for mixing aqueous fluids is consistent with those used in existing microfluidic devices.

The most direct experimental paper corresponding to the geometry of interest is the work of El Moctar *et al.* [14]. In their experiments, the permittivity of the buffer streams was dependent upon the frequency. In our comparison we focus on the regime where the frequency is sufficiently high such that the relative permittivity of the buffer streams is the same (see Fig. 3 of Ref. [14]). Using our analysis as in Fig. 2 we predict a critical voltage for observable instability and mixing to be approximately 18 V when we apply the parameters of their experiments. This predicted voltage is in range of their experiments, but lower than their reported 50 V threshold value for mixing. Their experimental setup had the additional effect that fluid is continuously pumped over the electrodes by external means. Therefore, to observe mixing we must consider whether the instability can grow to sufficient amplitude in the time that the fluid is between the electrodes.

Our model predicts that the maximum growth rate for El Moctar *et al.*'s experiments is $s=0.63$ at $k=5.2$. The amplification of a linear disturbance over the time fluid is between the electrodes can be computed as

$$A = e^{st_f U_{ev}/H}, \tag{43}$$

where t_f is the flow time between the electrodes and H/U_{ev} is the time scale used in the nondimensionalization. Using the experimental parameters we predict that a disturbance would amplify by a factor of $A=1000$ over the distance of the electrode at 70 V and a factor of $A=10\,000$ at 80 V. Such rapid linear growth rates at these voltages correspond to predictions of a well-mixed flow. Our theoretical predictions are consistent with the voltages used in experiments where good mixing was observed. Only simulations with nonlinear interactions can determine the mixing efficiency, however, our analysis from the linear stability problem provides a good estimate of the voltage needed for mixing.

In making our estimation we made a simplifying assumption that the Rayleigh number was very large while the Reynolds number remained small. The stability problem will only depend upon the conductivity ratio when we take the limits $\mathrm{Re}\to 0$ and $\mathrm{Ra}\to\infty$. We confirm that the experimental images provided in El Moctar *et al.* are well inside this regime. In microfluidic mixer applications where the Rayleigh numbers may be well above threshold to induce strong mixing of the fluid, this limit is accurate and simplifies the problem even further.

VI. CONCLUSIONS

Recent research has shown that electrohydrodynamic instabilities in microchannels can drive a low Reynolds number mixing flow. The instabilities hold promise as a passive mixing mechanism for microfluidic applications [14]. Our goal was to investigate the behavior of these instabilities when the driving electric forcing is time periodic. We explored an extensive range of parameter space, and have concluded that improving mixing by modulating the electric body force does not seem like a feasible strategy. In the regime where frequency dependence is found, the time scales of instability are so slow that molecular diffusion thoroughly mixes the fluids before instability sets in. The regimes of interest for mixing applications show that the ac case using the RMS voltage behaves the same as the dc case with no frequency dependence.

However, we found a strong frequency dependence when the base state of fluid electrical conductivity is considered steady. With the assumption of a steady base state, the flow can pass from stable to unstable by simple adjustment of the frequency. We expect that time periodic forcing would be important in configurations where conductivity gradients are permanent. A steady conductivity gradient can occur where the fluids are immiscible or the conductivity gradient is set by thermal or electrochemical effects. Such configurations are an area for future study.

While there are significant quantitative differences, qualitatively there is no significant difference in modeling the flow with the 2D equation set and the depth-averaged equation set. Both equation sets predict very similar results and similar features when viewed in Rayleigh number–wave number parameter space. This result indicates that, if full 3D modeling were conducted, we would not expect to find new behavior.

Experimental results of Shin *et al.* [17] showed a frequency-dependent mixing rate in unstable electrokinetic flow. In their experiments, they studied a thin layer of high conductivity fluid sandwiched between two low conductivity streams merged at a cross junction. The flow is driven by electro-osmosis. In their configuration, the flow is arranged such that the relative flow rates of the high and low conductivity fluid are periodic in time. In our study, it was only the

electric body force that was periodic in time. Based on our study it seems that the frequency dependence observed by Shin *et al.* [17] is likely due to modulating the flow rates. Variations on their scheme may hold promise for frequency-controlled mixing. Based on our results, mixing schemes that rely upon modulation of the electric body force do not seem to hold much promise as a method for improving fluid mixing.

ACKNOWLEDGMENT

This work was sponsored by the National Science Foundation, Grant No. CTS-0521845.

[1] D. R. Reyes, D. Iossifidis, P. A. Auroux, and A. Manz, Anal. Chem. **74**, 2623 (2002).
[2] S. Hardt, K. S. Drese, V. Hessel, and F. Schönfeld, Microfluid. Nanofluid. **1**, 108 (2005).
[3] J. M. Ottino and S. Wiggins, Philos. Trans. R. Soc. London, Ser. A **362**, 923 (2004).
[4] D. H. Michael and M. E. O'Neil, J. Fluid Mech. **45**, 571 (1969).
[5] G. I. Taylor and A. D. McEwan, J. Fluid Mech. **22**, 1 (1965).
[6] D. A. Saville, Annu. Rev. Fluid Mech. **29**, 27 (1997).
[7] J. F. Hoburg and J. R. Melcher, J. Fluid Mech. **73**, 333 (1976).
[8] J. F. Hoburg and J. R. Melcher, Phys. Fluids **20**, 903 (1977).
[9] J. R. Melcher and C. V. Smith, Phys. Fluids **12**, 778 (1969).
[10] J. R. Melcher, *Continuum Electromechanics* (MIT Press, Cambridge, 1981).
[11] J. C. Baygents and F. Baldessari, Phys. Fluids **10**, 301 (1998).
[12] H. Lin, B. D. Storey, M. H. Oddy, C. H. Chen, and J. G. Santiago, Phys. Fluids **16**, 1922 (2004).
[13] C.-H. Chen, H. Lin, S. K. Lele, and J. G. Santiago, J. Fluid Mech. **524**, 263 (2005).
[14] A. O. El Moctar, N. Aubry, and J. Batton, Lab Chip **3**, 273 (2003).
[15] B. D. Storey, Physica D **211**, 151 (2005).
[16] M. H. Oddy, J. G. Santiago, and J. C. Mikkelsen, Anal. Chem. **73**, 5822 (2001).
[17] S. M. Shin, I. S. Kang, and Y.-K. Cho, J. Micromech. Microeng. **15**, 455 (2005).
[18] A. T. Patera and B. B. Mikic, Int. J. Heat Mass Transfer **29**, 1127 (1986).
[19] N. K. Ghadar, K. Z. Korczak, B. B. Mikic, and A. T. Patera, J. Fluid Mech. **168**, 541 (1986).
[20] C. Von Kerczek and S. H. Davis, J. Fluid Mech. **62**, 753 (1974).
[21] V. Suresh and G. M. Homsy, Phys. Fluids **16**, 2349 (2005).
[22] M. H. Chang and G. M. Homsy, Phys. Fluids **17**, 074107 (2005).
[23] R. Probstein, *Physicochemical Hydrodynamics* (Wiley, New York, 1994).
[24] B. D. Storey, B. S. Tilley, H. Lin, and J. G. Santiago, Phys. Fluids **17**, 018103 (2005).
[25] H. Lin, B. D. Storey, and J. G. Santiago, in Proceedings of the International Mechanical Engineering Conference and Exposition 2004, Anaheim, IMECE2004–61017.
[26] V. Suresh, Ph.D. thesis, Stanford, 2002 (unpublished).
[27] L. Trefethen, *Spectral Methods in Matlab* (SIAM, Philadelphia, 2001).
[28] M. Z. Bazant, K. Thornton, and A. Ajdari, Phys. Rev. E **70**, 021506 (2004).
[29] S. S. Dukhin, Adv. Colloid Interface Sci. **35**, 173 (1991).
[30] E. K. Zholkovskij, M. A. Vorortynsev, and E. Staude, J. Colloid Interface Sci. **181**, 28 (1996).
[31] I. Rubinstein, B. Zaltzman, and I. Lerman, Phys. Rev. E **72**, 011505 (2005).
[32] M. Z. Bazant, M. S. Kilic, B. D. Storey, and A. Ajdari, e-print arXiv:cond-mat/0703035.